Exploring the Dynamics of Magnetic Fluctuations in Magnetite Nanoparticles

Daniel McPherson

A senior thesis submitted to the faculty of
Brigham Young University
in partial fulfillment of the requirements for the degree of

Bachelor of Science

Karine Chesnel, Advisor

Department of Physics and Astronomy

Brigham Young University

ABSTRACT

Exploring the Dynamics of Magnetic Fluctuations in Magnetite Nanoparticles

Daniel McPherson
Department of Physics and Astronomy, BYU
Bachelor of Science

Magnetic nanoparticles have a wide range of applications, from the engineering to the medical field. Understanding the properties of assemblies of magnetic nanoparticles is necessary to enhance the effectiveness of their use. A key feature of self-assemblies of magnetite nanoparticles is their superparamagnetic behavior. My current project focuses on understanding the dynamics of magnetic fluctuations in magnetite (Fe_3O_4) nanoparticles. The method of study is using x-ray resonant magnetic scattering (XRMS). We collected our XRMS data at SSRL. We study variations in the XRMS signal caused by assemblies of magnetite nanoparticles. A certain amount of data refinement is necessary to isolate the coherent x-ray scattering signal, also known as magnetic speckle. Upon isolation of coherent signal, speckle patterns collected throughout 1000 second periods are cross-correlated in order to study the magnetic fluctuation dynamics. We compare two-time cross-correlation maps collected at different temperatures cross-correlation throughout the superparamagnetic blocking transition.

Keywords: Magnetite, Cross-Correlation, Blocking Transition, Characteristic Time, Nanoparticles

ACKNOWLEDGMENTS

I would like to thank my wife Vanese for her understanding and support through every moment that enabled this research to happen. I would also like to thank the numerous faculty and staff at Brigham Young University for their tireless efforts in enabling students to succeed. Finally, special thanks to my research advisor Dr. Karine Chesnel for superb direction and advise that has shaped the process herein.

Contents

Chapter 1

Introduction

1.1 Nanoparticle Applications

Magnetic nanoparticles have a wide variety of biopharma applications, such as MRI contrast agent, cellular compound delivery, and localized hyperthermia. Magnetite nanoparticles were chosen for this study in part because they are non-toxic which is necessary for biomedical applications; they can also be functionalized for molecule and drug targeting applications. Nanoparticles have also been successfully used as contrasting agent in MRIs [1]. Because their size is comparable to the 50 nm nuclear pore, the nanoparticles can be used to deliver compounds into targeted locations [2] [3]. Nanoparticles have also been used to heat up localized tissue (hyperthermia). The ability to selectively heat up cell groupings has applications in cancer treatment [2]. Nanoparticles exhibit a variety of behaviors under variable conditions such as temperature or external magnetic field. Understanding how nanoparticles behave with varying temperature and magnetic field is useful for implementing all these applications.

1.2 Sample Characteristics

For this study we are examining magnetite (Fe_3O_4) nanoparticles. Other related studies of this material by our group are reported in [4] [5]. The nanoparticles were fabricated in collaboration with the BYU chemistry department. The Fe_3O_4 nanoparticles have a combination of Fe^{+3} and Fe^{+2} ions; these ions are arranged ferrimagnetically throughout the crystallographic structure; thus creating a nanospin at the scale of the nanoparticle. When a collection of such nanospin is formed, they often exhibit superparamagnetism.

As mentioned previously, better understanding nanoparticle properties is an important step in expediting their use. One such property is the dynamics of magnetic fluctuation in the magnetite nanoparticle self-assemblies. The rate of fluctuation of the nanomagnetic spin is represented by the characteristic time (t). This characteristic time is a measure of the average time for a nanospin to fluctuate. The blocking temperature is the temperature when the characteristic time the measurement time. In our study, the data was collected on a CCD camera so the measurement time assimilates to the CCD exposure time, which was 20 seconds. The blocking temperature estimated on magnetometry measurements (collected at a rate of 1 seconds) for 11 nm nanoparticles is 170 K. At temperatures below the blocking temperature, the nanoparticles self-assemblies average fluctuation time is greater then 20 seconds. We are particularly interested in following the dynamics of fluctuation as the sample warms through the blocking temperature. An image of the sample under study can be seen in the transmission electron microscopy (TEM) image in Fig. 1.1. We here examine how the particle self-assembly behavior evolves while warming through the blocking temperature in the absence of an external field.

TEM image of magnetite nanoparticles

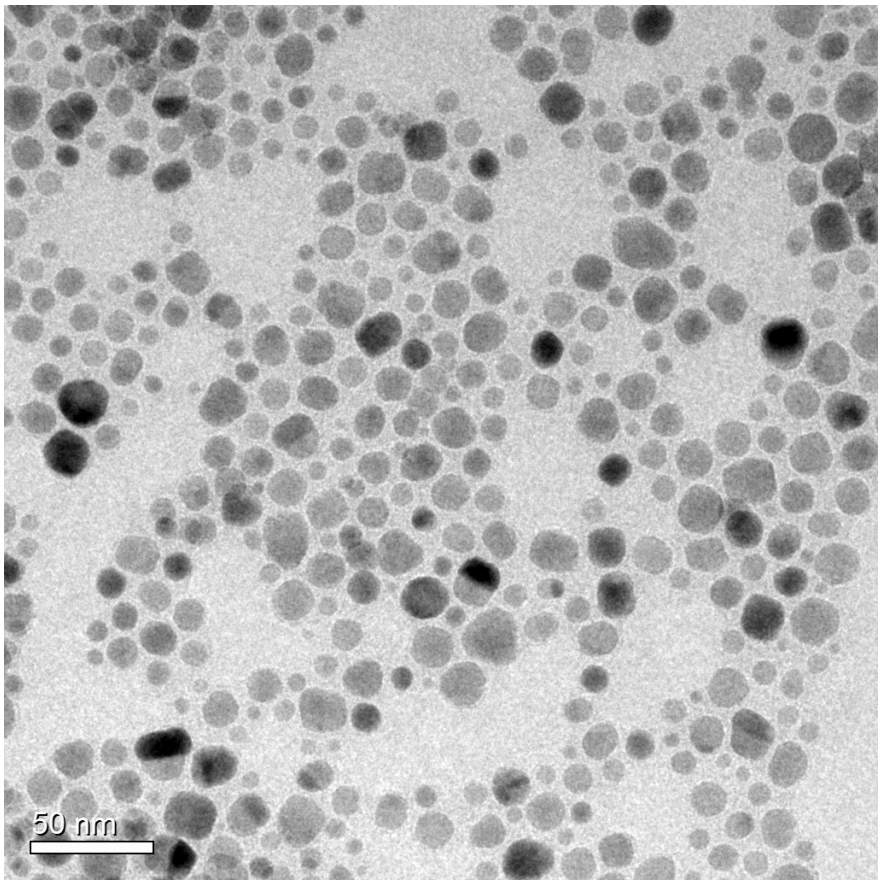

Figure 1.1 11 nm on average sample, the focus if this study. The sample was fabricated with collaboration from the BYU chemistry department.

1.3 Research Objective

The objective of this study is to quantify spin fluctuation in the nanoparticle self-assembly as a function of time and temperature. Photon cross-correlation metrology is a technique allowing to follow nanoscopic variations in a material either over time [6] [7] or as a function of field cycling [8]. here, we likewise utilize cross-correlation but in this case to study nanomagnetic spin fluctuations in magnetite nanoparticle self-assemblies. In order to reduce computation time, we developed a set of analysis programs to carry out the cross-correlation, either via pixel-by-pixel multiplication approach (see section 2.3.1) or by using Fast Fourier Transforms (see section 2.3.2) [8] [9]. Using Fourier transforms to compute cross-correlations is quick and computationally inexpensive. Once all images were cross-correlated, the correlation drop over time during the span of 1000 seconds was examined. In this study, the time is controlled but the temperature was allowed to increase freely 105 K to 262 K. To our knowledge no such study as been conducted before. The motivation for this experiment was that the results were as yet untested. The two methods of cross-correlation, Fourier based and pixel-by-pixel, provide a unique opportunity to compare the results of different methodologies.

1.4 Previous Work

The scattering data used for this study were collected previously at the Stanford Synchrotron Radiation Lightsource (SSRL). X-rays were tuned to the absorption edge for Fe -L_3. The energy of the absorption edge was 708 eV as described in [10]. The tuned resonant x-rays were used to provide magnetic contrast from the Fe carried spin in Fe_3O_4. A general depiction of the experimental setup can be seen in Fig. 1.2. The coherent x-ray been was focused down to approximately 70 microns. The sample consisted of an monolayer of magnetite nanoparticles. A CCD camera was used for image collection. The scattering signal has two contributions to it: Charge scattering, and magnetic

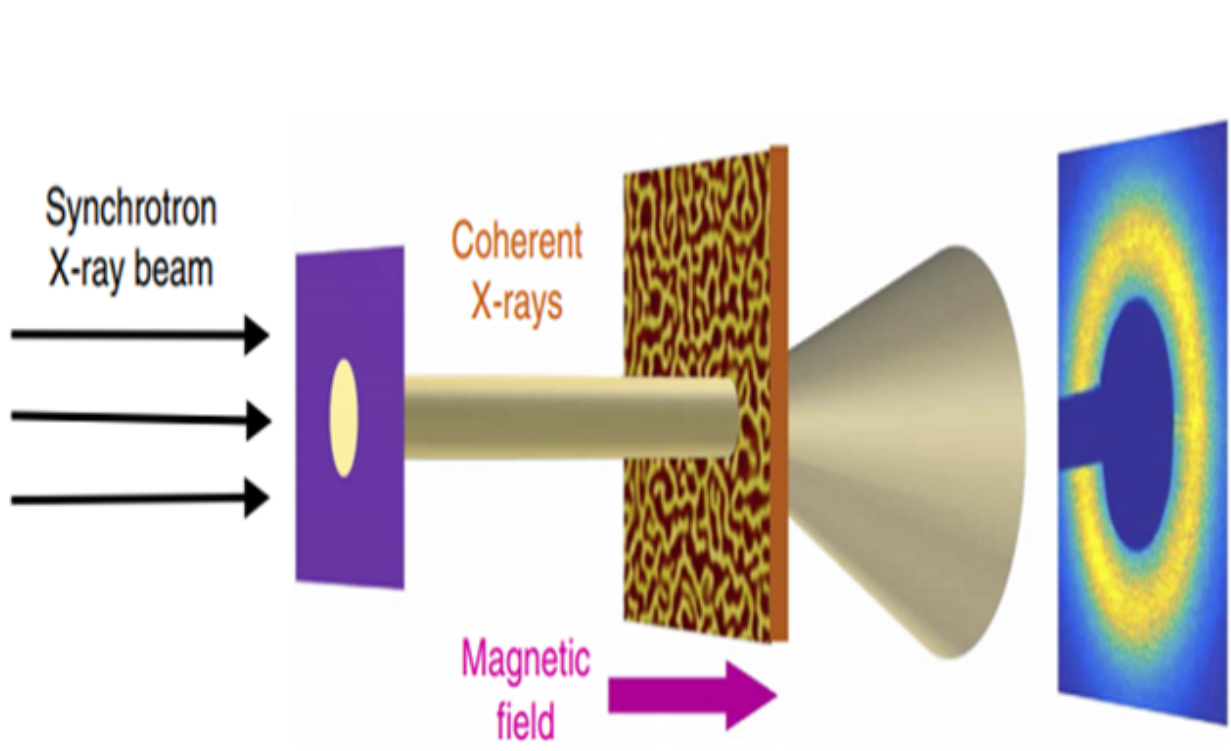

Figure 1.2 General components for the SSRL beam line experiment.

scattering signal. Because the light used was coherent, part of the scattering pattern was also coherent. The coherent portion of the signal is referred to as the 'speckle'. The image in Fig. 1.4 is the raw signal taken at the detector. The ring shape visible in the image arises from the incoherent signal; it comes from the long range order of the sample. The size of the observed ring is inversely proportional to the inter-particle distance within the sample [10]. The speckle in contrast, is related to the disorder within the sample. A representative sampling of the magnetite nanoparticles used can be seen in Fig. 1.1. As can be seen in the figure some variation in particle size is present. For this study I created part of the cross-correlation code. Some of the analysis tools used for the Fourier method described below was created in previous studies. [11] [12]

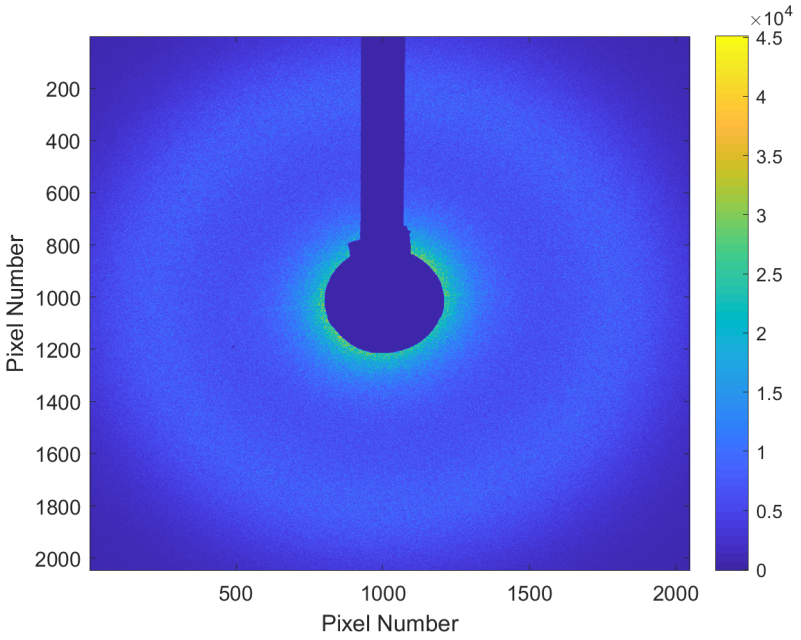

Figure 1.3 Raw image of magnetic x-ray scattering. The blocker shielding the CCD can be seen at the image top and center. The color bar on the right is a unitless photon count measure.

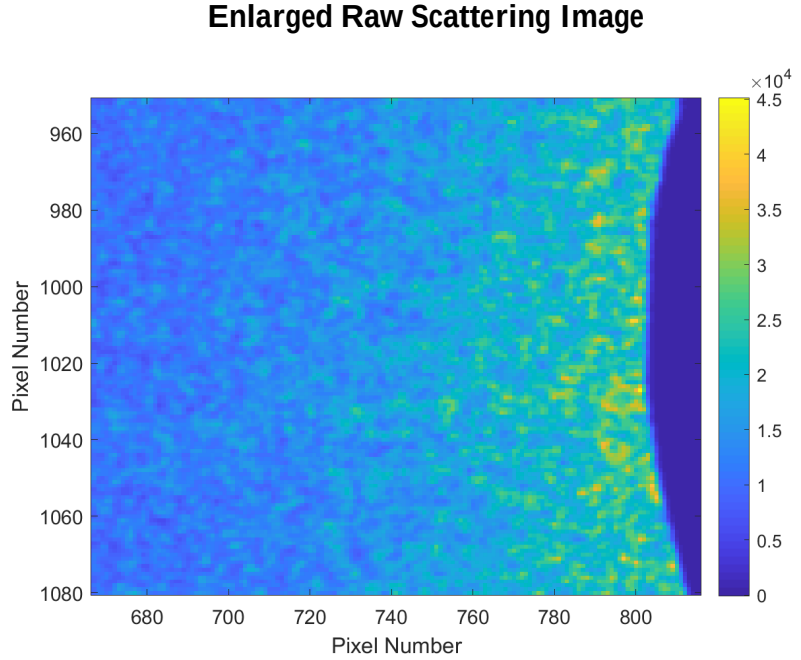

Figure 1.4 Raw image of magnetic x-ray scattering. The color bar on the right is a unitless photon count measure. Speckles can be seen in this enlarged image.

Chapter 2

Methods

2.1 Data Description

The scattering images used for this study were 2048 by 2048 pixel. Images such as the one shown in Fig. 1.4 were collected in sets of 50 images with a 20 second exposure time each, for a total time of about 1000 seconds. In total twenty five of such sets were collected, at various temperatures form about 105 K up to about 263 K. The images in this study were collected as part of a warming-up study where the sample had already bean cooled well below the blocking temperature. The sample was allowed to warm through the 170 K blocking temperature from 105 K to 262 K with no applied field.

2.2 Magnetic Speckle Extraction

In order to isolate the coherent signal, the data collected was iteratively averaged to produce a two-dimensional "envelope" signal. This envelope signal corresponds to what would be measured with totally incoherent light. The iterative smoothing process was carried out by averaging neighboring points. At each smoothing pass the second derivative of the residual between the raw data and the

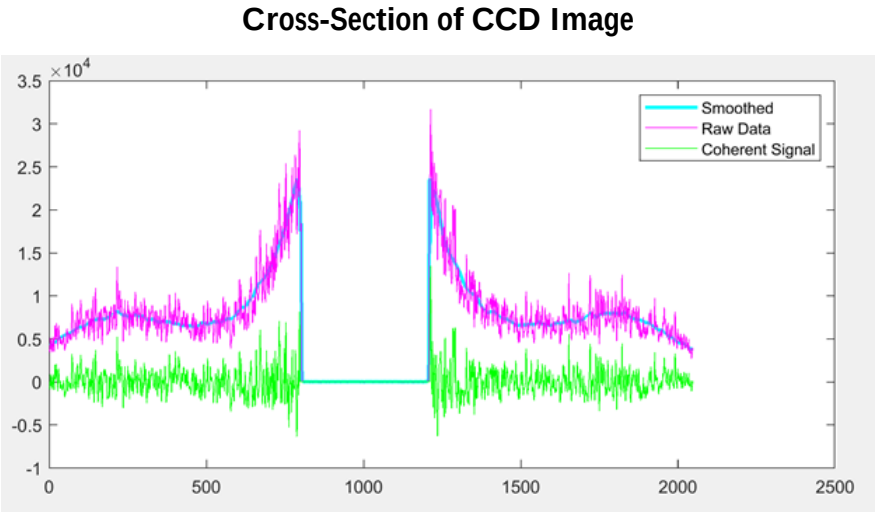

Figure 2.1 A slice through image center with photon counts plotted on the y-axis. The blue smoothed line is the incoherent envelope subtracted from the raw image to isolate the coherent signal.

envelope was calculated and compared to the prescribed tolerance. The smoothing continued until the second derivative fell below the designated tolerance value yielding the incoherent envelope. The incoherent envelope was then subtracted from the raw image leaving the a residual, which is essentially the coherent signal. Fig. 2.1 illustrates the smoothing process components. Smoothing tolerances from 0.1 to 0.001 were tested, and an optimal tolerance of 0.01 was determined for coherent signal isolation. The coherent signal is related to the self-assembly and is used to explore the dynamics of magnetic fluctuations that may exist in the system.

2.3 Cross-Correlation

Upon isolation of the coherent signal, we cross correlate speckle patterns collected at different times to monitor the dynamics of magnetic fluctuations. The general formula for two-dimensional cross-correlation is:

$$C_{AB}(u;v) = \int_{-\infty}^{\infty}\int_{-\infty}^{\infty} A(x;y)\ B(u-x;v-y)dxdy; \tag{2.1}$$

Where A, and B are two-dimensional matrices representing the speckle patterns. $C_{AB}(u;v)$ is the correlation pattern produced by the cross-correlation of A and B or: the convolution of $A((x;y)$ and $B(u \quad x;v \quad y)$, with u and v being the amount of shift applied to one pattern in respect to the other one. In the case of $A = B$ the result is an auto-correlation. To compute equation 2.1 we used two methods described below. Once the cross-correlation was computed, we calculated a normalized cross-correlation coefficient r:

$$r = \frac{SC_{AB}(u;v)}{\sqrt{SC_{AA}(u;v)^2 SC_{BB}(u;v)^2}} \tag{2.2}$$

Where $C_{AB}(u;v)$ is the cross-correlation pattern of image A and B with indices u, and v. $C_{AA}(u;v)$ is the auto-correlation of image A and $C_{BB}(u;v)$ is the auto-correlation pattern of image B and S represents the summation of all the pixels in these patterns- necessary in the second method only. We will see below how the second method offers the possibility to track any experimental sample shifting throughout the measurement. By cross correlating images of the magnetite sample, the resulting correlation map can be used to determine how quickly the magnetite self-assemblies are changing with time.

2.3.1 Method 1

The first method is based on a built-in function in MATLAB©, called *Corr2*. *Corr2* is a simple and fast two dimensional cross-correlation method. *Corr2*, unlike a true cross-correlation it will not compensate for any experimental sample or detector drifting. The first method takes the isolated coherent signal and uses *Corr2* to cross-correlate the speckle patterns. This function utilizes a pixel-by-pixel multiplication approach to produce a normalized coefficient of correlation using the following equation to find the scalar degree of correlation r, with values between 0 and 1.

$$r = \frac{S_m S_n (A_{mn} \quad \bar{A})(B_{mn} \quad \bar{B})}{\sqrt{S_m S_n (A_{mn} \quad \bar{A})^2 \quad S_m S_n (B_{mn} \quad \bar{B})^2}}: \tag{2.3}$$

Where A_{mn} are the m by n element of speckle image A, and $\bar{A}$ is the average value of image A. Likewise, B_{mn} are the m by n element of speckle pattern B, and $\bar{B}$ is the average value of image B. The correlation coefficient was mapped for each set of 50 images into a two-time correlation map as depicted in Fig. 2.3.

2.3.2 Method 2

The second method utilized FFT cross-correlation, and is a true cross-correlation equivalent to equation 2.1. The use of FFT allows for faster computing compared to the simplified pixel-by-pixel approach used for method one. The Fourier based cross-correlation takes the form of:

$$C_{AB}(u;v) = \mathscr{F}^{-1}\{\mathscr{F}[A(x;y)] \quad \mathscr{F}[B(\quad x: \quad y)]\} \tag{2.4}$$

Where $\mathscr{F}$ is the two-dimensional Fourier transform and $\mathscr{F}^{-1}$ is the inverse two-dimensional Fourier transform. The coordinate $\quad x$, and $\quad y$ for image B represent a 180 rotation necessary for the correlation operation. The " " in the above equation represents scalar pixel multiplication. $C_{AB}(u;v)$ is the cross-correlation pattern of A and B with indices u and v. Operation 2.4, unlike 2.1 can be computed rapidly, but is still equivalent to 2.1 and results in a correlation peak as depicted in Fig. 2.2. For nearly all data sets, the correlation peak experienced some amount of drifting over time as described below. When the cross-correlation operation of equation 2.4 is completed, the peak in the correlation pattern was observed to shift from the image center. This shifting is shown in section 3.3. All cross-correlations except auto-correlations experienced some amount of drifting over time. During the FFT method each correlation peak was recentered with the peak at the origin; this correction took place as part of the correlation process. The peak was then integrated over an ellispe area with diameter of about two times the FWHM of the peak. This would correspond to a typical ellipse radius of five pixels. The integration results for each correlation pair was then normalized using equation 2.2.

Subsequently these normalized values were arranged in a two-time correlation map such as 2.4.

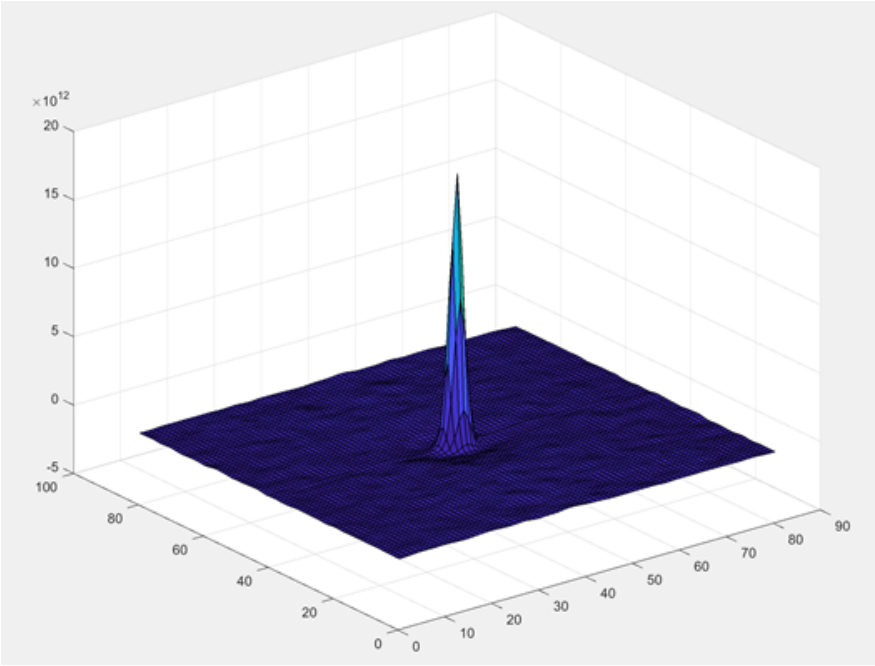

Figure 2.2 Correlation pattern produced using cross-correlation equation 2.4.

2.4 Two-Time Correlation Maps

Upon cross-correlation completion both methods produced 25 sets of 50 50 = 2500 values for r. Each set mapped in two-time space. On such a correlation, map, an idex (m,n) corresponded to image taken at 20 m seconds cross-correlated with image taken at 20 n seconds. Fig. 2.3, and Fig. 2.4 are sample maps using method one and method two respectively. By symmetry, the two halves of the correlation matrix reflect each other. Only the center diagonal which corresponds to the auto-correlation is unique. The total number of unique data points is then 1225 + 50 in each set.

2.5 One-Time Correlation Plot

Each two-time correlation map was reduced to a one-time correlation plot. The one-time plots were created by averaging pixels that had the same index difference (m-n), that is, the time lag between correlated images. Once average correlation values for the 50 unique (m-n) time lags were

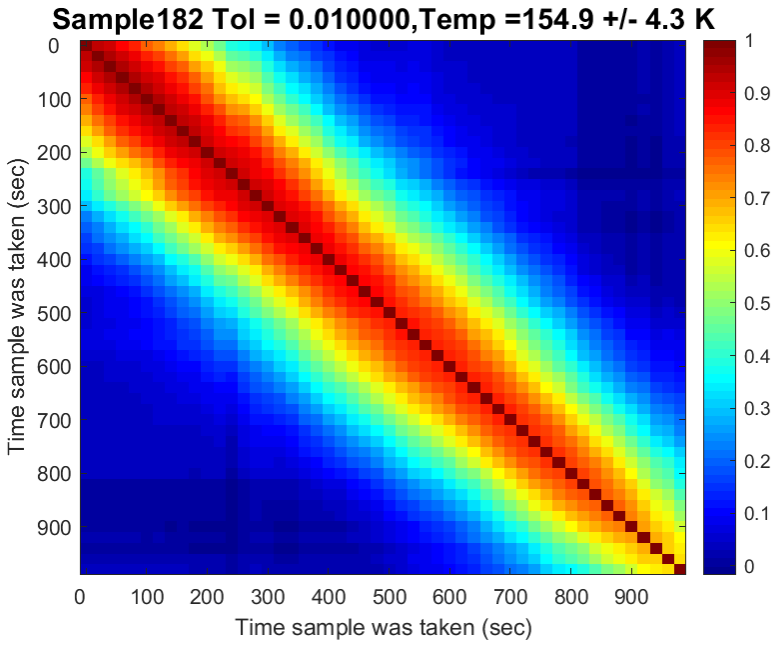

Figure 2.3 Plot showing two-time maps generated using MATLAB built in *Corr2* pixel-by-pixel correlation method. The colorbar indicates correlation coefficient

Figure 2.4 Plot showing two-time maps generated using Fourier correlation method of equation 2.4. The colorbar indicates correlation coefficient

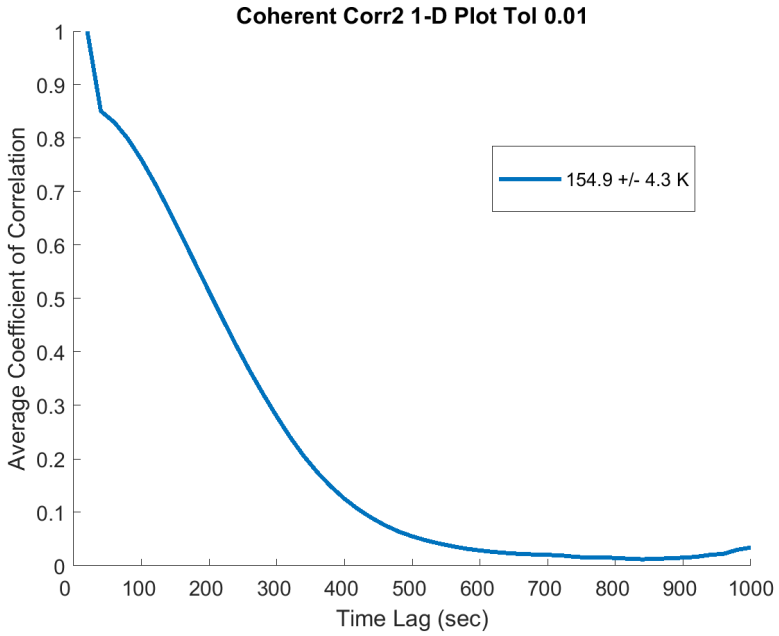

Figure 2.5 One dimensional plot of average correlation coefficient from *Corr2* method.

calculated, a plot of the average correlation value as a function of time lag between images was generated. A sampling of these one-time plots can be seen in Fig. 2.5

2.6 Characteristic Time of Fluctuation

Creating one-dimensional plots allows for fitting to an exponential decay function of the form:

$$r(t) = r(0)e^{t=t} \tag{2.5}$$

Where $r(0)$ is the amplitude, t is the time, and t is the characteristic time. Our data generally showed such a behavior with rho (t) decreasing over time. By plotting t as a function of temperature it is possible to determine possible phase transitions. Our data showed a trend counter to expectation; subsequently, the temperature variation throughout each 1000 second measurement was plotted against the observed drop in correlation. The goal for plotting correlation drop against temperature was to determine factors that may have contributed to the observed outcome.

Chapter 3

Results

3.1 Two-Time Correlation Maps

In order to understand how the magnetite nanoparticles behave over time with increasing temperature, two-time maps generated from an array of correlation coefficients were created. The two-time maps using the pixel-by-pixel multiplication approach are displayed in appendix A. Two-time maps generated using the Fourier based cross-correlation are displayed in appendix B. Each two-time map consolidates data from each 1000 second set into one visual. It should be noted that maps found in appendix B showed a rougher correlation pattern for reasons we are still investigating.

3.2 One-Dimensional Plots

In order to isolate the time evolution of nanoparticle assemblies, one dimensional plots averaging correlation coefficient as a function of time between correlation images were generated and can be seen in Fig. 3.1, Fig. 3.2, and Fig. 3.3. Fig. 3.1 is a representative sample of one dimensional maps generated using the corr2 approach. Fig. 3.2, and Fig. 3.3 are respectively at the beginning and end of the blocking transition cross-correlated using the FFT method.

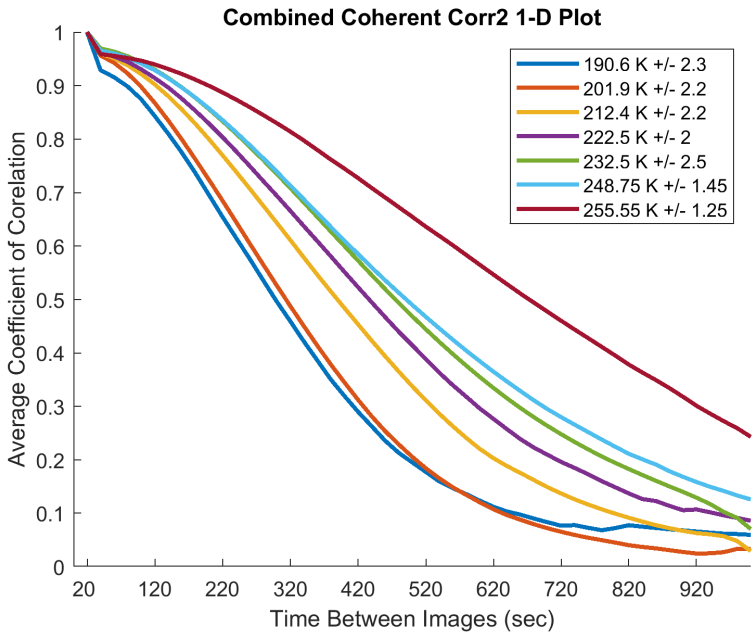

Figure 3.1 A selection of one dimensional plots of average correlation coefficient from *Corr2* method.

Figure 3.2 One dimensional plot of average correlation coefficient from FFT correlation method.

Figure 3.3 One dimensional plot of average correlation coefficient from FFT correlation method.

3.3 Comparison Between Methods and Drifting Effects

It can be seen when comparing one-dimensional plots for the *Corr2* and the FFT method that significant differences exists. In the *Corr2* method plots such as Fig. 2.5, we see smooth plots that reach a near zero correlation value after 1000 seconds. In the FFT method such as Fig. 3.2 and 3.3, the plots are rough and the correlation coefficient is above 0.7 after 1000 seconds. To investigate the cause of this discrepancy in cross-correlation between the two methods, the possible drifting effects were explored by tracking the position of the correlation peak in Method 2. A peak shifting is generally caused by instrumental noise, leading to gradual displacement of the sample position in respect to to the x-ray beam and the detector. Consequently, the position of the speckle spots on the detector, and speckle pattern as a whole, are gradually shifting, causing in turn the correlation peak to shift the same amount of pixels. If the peak shifting is not properly compensated, it may cause an artificial loss in the correlation number. Method 1 did not compensate for sample motion.

Figure 3.4 Tracking of peak motion in each 50 image cross-correlation set. The blue line outlines the integration ellipse. The orange line tracks the peak of the correlation pattern.

By plotting the correlation peak we obtain an idea of how much shifting occurred. Fig. 3.4 is an example plot showing how the correlation peak shifts over time. Peak shifting for all the data sets can be seen in appendix D. We see that for the lower temperature cross-correlations, the peak shifts by a greater distance, even reaching outside of the integration ellipse. The shifting behavior point to the possibility of large scale sample motion not accounted for in the *Corr2* method. Which would then explain the significantly bigger drop in correlation, even all the way down to zero at the lower temperatures.

3.4 Characteristic Time Fits

Exponential decay fits using equation 2.5 were attempted for a selection of one dimensional plots using the *Corr2* method and can be seen in Fig. 3.5. From cursory evaluation it was apparent that while at lower temperature a reasonable fit can be achieved; at higher temperatures it is apparent that the exponential decay function poorly models the observed behavior. Additionally, a trend was observed where the correlation drop at higher temperatures was lower then at lower temperatures; Ordinarily upon generating figures such as Fig. 3.1, Fig. 3.2, and Fig. 3.3 characteristic time would be estimated by fitting an exponential decay functions like equation 2.5, from which the characteristic time could be determined for Fig. 3.2, and Fig. 3.3. more data refinement is necessary for determining an accurate characteristic time. Upon examination of Fig. 3.1, it is noticeable that with increasing temperature the slope becomes more shallow. A shallower slope corresponds to a decrease in thermal fluctuations; this observed trend is opposite to what is expected when transitioning from a blocked state to a superparamagnetic state and cast doubt on the validity of static pixel-by-pixel correlation methods. While plots generated using the Fourier space correlation have a high level of noise, they nevertheless show a trend closer to the expected general trend. However, neither methods follows the expected slope trend to be conclusive. In Fig. 3.2 a strong plateauing behavior can be seen at lower temperatures. In Fig. 3.3 the plateauing has nearly stopped giving way to a scattered downward arc. Unlike trends observed from the *Corr2* analysis in Fig. 3.1 the general trend observed from the Fourier correlation method follows general trends consistent with thermal fluctuation increases with increasing temperature in some instances but not all. The correlation drop $\Delta r = r_{50} - r_2$ from beginning to end of each set is shown in Fig. 3.7 for the *Corr2* method and in Fig. 3.6 is the Fourier based approach. The trend is noisy but somewhat opposite to what is expected. The reason may be due to the unstable temperature during the data collection: the temperature variation was larger at low T and smaller at high T. This temperature variation may overcome the variations due to actual magnetic fluctuations.

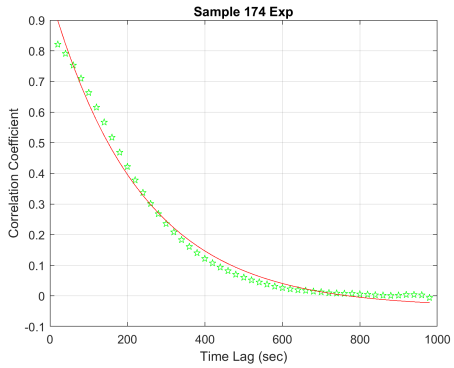

(a) Exponential Fit Average Temp of 110 K +/- 5 K

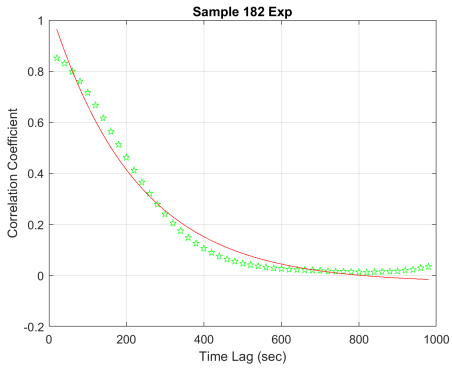

(b) Exponential Fit Average Temp of 154.9 K +/- 3.65 K

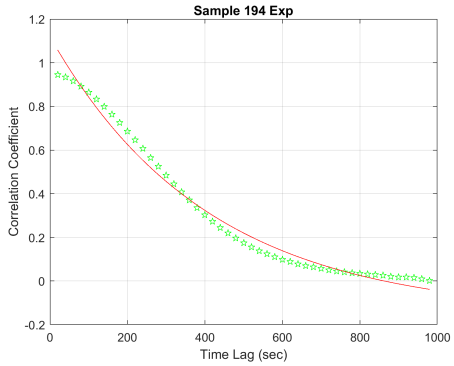

(c) Exponential Fit Average Temp of 196.05 K +/- 2.25 K

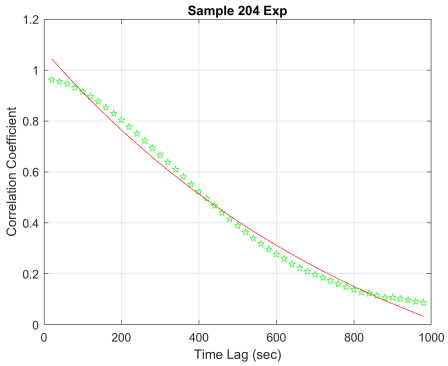

(d) Exponential Fit Average Temp of 222.5 K +/- 2 K

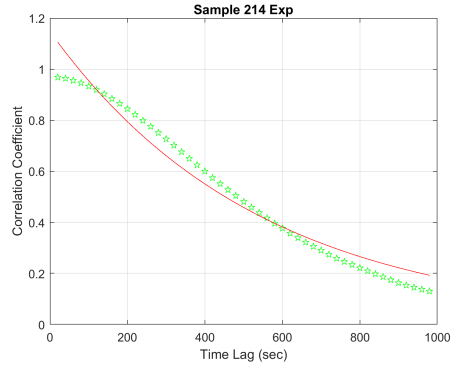

(e) Exponential Fit Average Temp of 244.5 K +/- 1.7 K

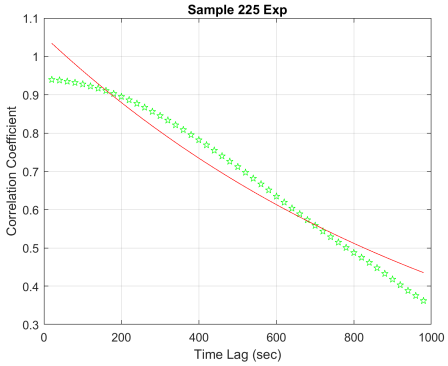

(f) Exponential Fit Average Temp of 261.2 K +/- 1.1 K

Figure 3.5 Exponential fit for one dimensional correlation plots produced with Corr2. Green stars represent data point for the correlation process and the red line is the best fit using exponential decay.

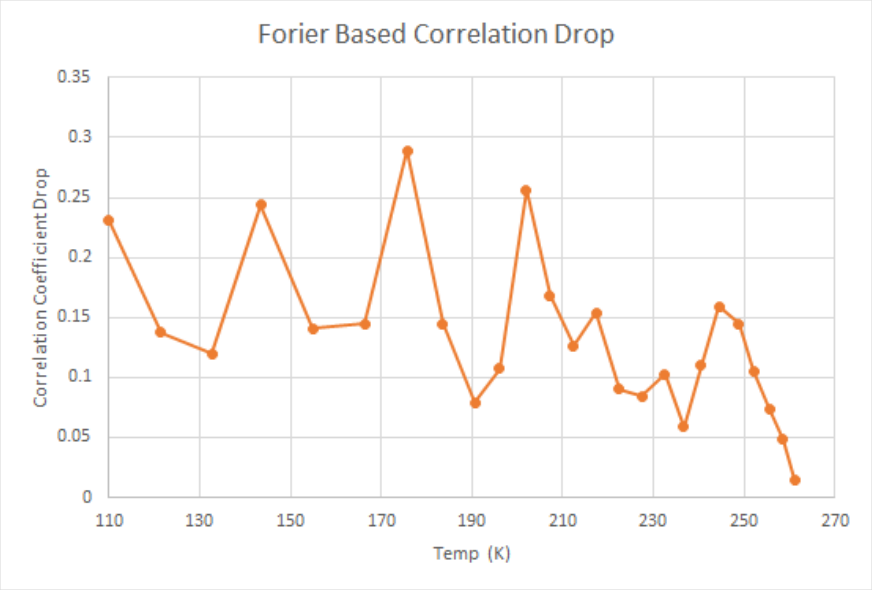

Figure 3.6 Each point represents correlation drop across 1000 second range for Fig. 3.2 and 3.3. The correlation drop is plotted against the average temperature that each data set was taken at. Correlation plot for the FFT method with tolerance of 0.01.

3.5 Future Work

A primary concern with using a Fourier correlation method is the roughness of the resulting correlation plot. Addressing this roughness is one of our primary goals in future work. Additionally, the unexpected behavior as a function of temperature observed still needs to be interpreted. Indeed, as indicated in both Fig. 3.6 and Fig. 3.7, we observed that the correlation drop over 1000 sec, was overall decreasing when temperature increased. As mentioned earlier this trend is counterintuitive. We suggest that this trend may be due to temperature instability being greater at low temperature compared to higher temperature, as illustrated in Fig. 3.8. Further investigations may be needed to verify if these trends are indeed correlated.

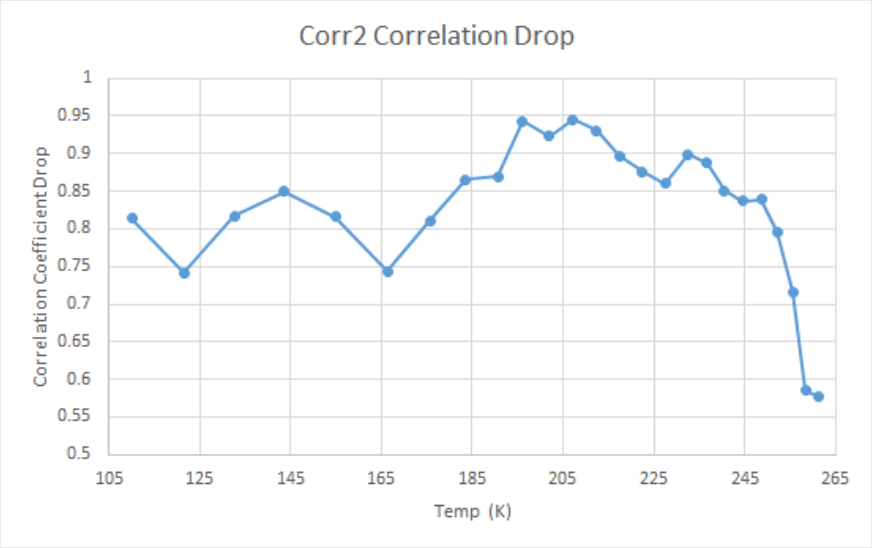

Figure 3.7 Plot showing correlation drop as a function of average temperature during through 1000 second interval for Corr2 based correlation method.

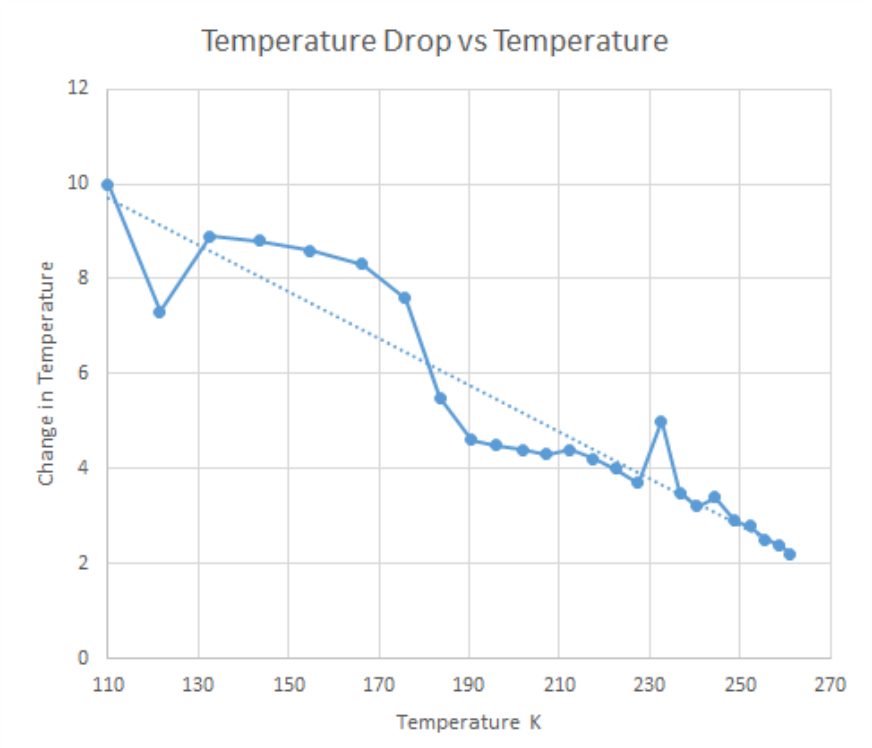

Figure 3.8 Plot showing the change in temperature for each measurement set as a function of the average temperature.

List of Figures

Index

Appendix A

Corr2 two-time maps

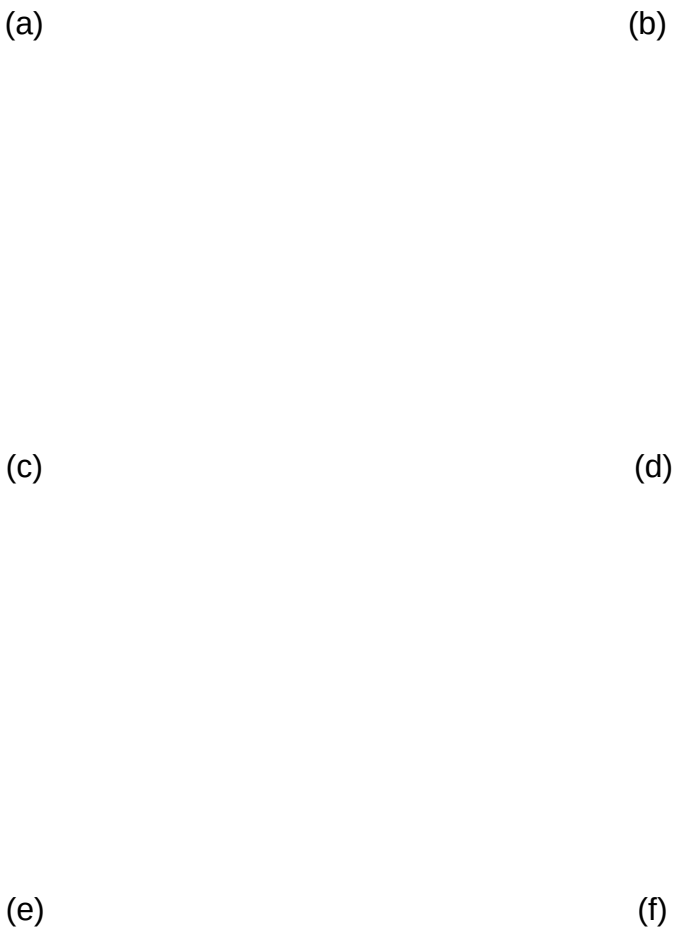

Figure A.1 Two-time correlation maps generated by pixel-by-pixel multiplication method Corr2. Maps for temperatures from 105 to 170.5 K. The colorbar indicates the correlation coef cient. Tolerance used for isolating coherent signal was 0.01.

(a) (b)

(c) (d)

(e) (f)

Figure A.2 Two-time correlation maps generated by pixel-by-pixel multiplication method Corr2. Maps for temperatures from 172 to 209.3 K. The colorbar indicates the correlation coef cient. Tolerance used for isolating coherent signal was 0.01.

(a) (b)

(c) (d)

(e) (f)

Figure A.3 Two-time correlation maps generated by pixel-by-pixel multiplication method Corr2. Maps for temperatures from 210.2 to 238.5 K. The colorbar indicates the correlation coef cient. Tolerance used for isolating coherent signal was 0.01.

(a) (b)

(c) (d)

Figure A.4 Two-time correlation maps generated by pixel-by-pixel multiplication method Corr2. Maps for temperatures from 238.9 to 253.6 K. The colorbar indicates the correlation coef cient. Tolerance used for isolating coherent signal was 0.01.

(a) (b)

(c)

Figure A.5 Two-time correlation maps generated by pixel-by-pixel multiplication method Corr2. Maps for temperatures from 254.3 to 262.3 K. The colorbar indicates the correlation coef cient. Tolerance used for isolating coherent signal was 0.01.

Appendix B

Fourier based correlation two-time maps

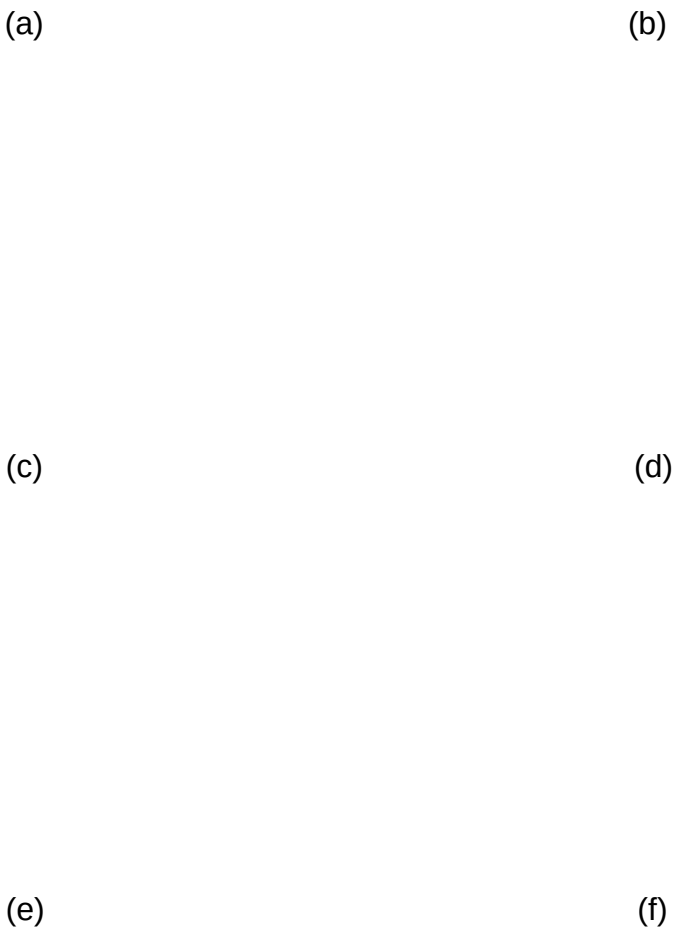

Figure B.1 Two-time correlation maps generated by Fourier based method. Maps for temperatures from 105 to 170.5 K. The colorbar indicates the correlation coef cient. Tolerance used for isolating coherent signal was 0.01.

(a) (b)

(c) (d)

(e) (f)

Figure B.2 Two-time correlation maps generated by Fourier based method. Maps for temperatures from 172 to 209.3 K. The colorbar indicates the correlation coef cient. Tolerance used for isolating coherent signal was 0.01.

(a) (b)

(c) (d)

(e) (f)

Figure B.3 Two-time correlation maps generated by Fourier based method. Maps for temperatures from 210.2 to 238.5 K. The colorbar indicates the correlation coef cient. Tolerance used for isolating coherent signal was 0.01.

(a) (b)

(c) (d)

Figure B.4 Two-time correlation maps generated by Fourier based method. Maps for temperatures from 238.9 to 253.6 K. The colorbar indicates the correlation coef cient. Tolerance used for isolating coherent signal was 0.01.

(a) (b)

(c)

Figure B.5 Two-time correlation maps generated by Fourier based method. Maps for temperatures from 254.3 to 262.3 K. The colorbar indicates the correlation coef cient. Tolerance used for isolating coherent signal was 0.01.

Appendix C

One-Time Correlation Plots

(a) (b)

(c) (d)

Figure C.1 One-dimensional plots of average coef cient of correlation as a function of temperature for the pixel-by-pixel multiplication approach. Tolerance used for isolating coherent signal was 0.01.

(a) (b)

(c) (d)

Figure C.2 One-dimensional plots of average coef cient of correlation as a function of temperature for the FFT based approach. Tolerance used for isolating coherent signal was 0.01.

Appendix D

Peak Shift Plots

(a) (b)

(c) (d)

Figure D.1 Tracking of peak motion in each 50 image cross-correlation set. The blue line outlines the integration ellipse. The orange line tracks the peak of the correlation pattern.

(a) (b)

(c) (d)

Figure D.2 Tracking of peak motion in each 50 image cross-correlation set. The blue line outlines the integration ellipse. The orange line tracks the peak of the correlation pattern.

(a) (b)

(c) (d)

Figure D.3 Tracking of peak motion in each 50 image cross-correlation set. The blue line outlines the integration ellipse. The orange line tracks the peak of the correlation pattern.

(a) (b)

(c) (d)

Figure D.4 Tracking of peak motion in each 50 image cross-correlation set. The blue line outlines the integration ellipse. The orange line tracks the peak of the correlation pattern.

(a) (b)

(c) (d)

Figure D.5 Tracking of peak motion in each 50 image cross-correlation set. The blue line outlines the integration ellipse. The orange line tracks the peak of the correlation pattern.

(a) (b)

(c) (d)

Figure D.6 Tracking of peak motion in each 50 image cross-correlation set. The blue line outlines the integration ellipse. The orange line tracks the peak of the correlation pattern.

Figure D.7 Tracking of peak motion in each 50 image cross-correlation set. The blue line outlines the integration ellipse. The orange line tracks the peak of the correlation pattern.

Bibliography

[1] E. Duguet, S. Vasseur, S. Mornet, and J.-M. Devoisselle, “Magnetic nanoparticles and their applications in medicine,” (2006).

[2] N. A. Frey, S. Peng, K. Cheng, and S. Sun, “Magnetic nanoparticles: synthesis, functionalization, and applications in bioimaging and magnetic energy storage,” Chemical Society Reviews 38, 2532–2542 (2009).

[3] V. Mohanraj and Y. Chen, “Nanoparticles-a review,” Tropical journal of pharmaceutical research 5, 561–573 (2006).

[4] S. Klomp, C. Walker, M. Christiansen, B. Newbold, D. Griner, Y. Cai, P. Minson, J. Farrer, S. Smith, and B. J. Campbell, “Size-Dependent Crystalline and Magnetic Properties of 5–100 nm Fe_3O_4 Nanoparticles: Superparamagnetism, Verwey Transition, and FeO–Fe_3O_4 Core–Shell Formation,” IEEE Transactions on Magnetics 56, 1–9 (2020).

[5] J. Rackham, B. Newbold, S. Kotter, D. Smith, D. Griner, R. Harrison, A. H. Reid, M. Transtrum, and K. Chesnel, “Modeling inter-particle magnetic correlations in magnetite nanoparticle assemblies using x-ray magnetic scattering data,” AIP Advances 9, 035033 (2019).

[6] D. K. Saldin, H. C. Poon, M. J. Bogan, S. Marchesini, D. A. Shapiro, R. A. Kirian, U. Weierstall, and J. C. H. Spence, “New Light on Disordered Ensembles: Ab Initio Structure

Determination of One Particle from Scattering Fluctuations of Many Copies," Physical Review Letters **106,** 115501 (2011).

[7] B. Pedrini, A. Menzel, M. Guizar-Sicairos, V. A. Guzenko, S. Gorelick, C. David, B. D. Patterson, and R. Abela, "Two-dimensional structure from random multiparticle X-ray scattering images using cross-correlations," Nature communications **4,** 1–9 (2013).

[8] K. Chesnel, A. Safsten, M. Rytting, and E. E. Fullerton, "Shaping nanoscale magnetic domain memory in exchange-coupled ferromagnets by field cooling," Nature communications **7,** 1–8 (2016).

[9] K. Chesnel, B. Wilcken, M. Rytting, S. D. Kevan, and E. E. Fullerton, "Field mapping and temperature dependence of magnetic domain memory induced by exchange couplings," New Journal of Physics **15,** 023016 (2013).

[10] K. Chesnel, D. Griner, D. Smith, Y. Cai, M. Trevino, B. Newbold, T. Wang, T. Liu, E. Jal, and A. H. Reid, "Unraveling nanoscale magnetic ordering in Fe3O4 nanoparticle assemblies via x-rays," Magnetochemistry **4,** 42 (2018).

[11] A. Safsten, Senior thesis, 2015.

[12] B. Wilcken, Senior thesis, 2009.